Full Text View

Volume 30, Issue 8 (August 2000)

Journal of Physical Oceanography
Article: pp. 2013–2034 | Abstract | PDF (494K)

On the Relationship of the Circumpolar Current to Southern Hemisphere Winds in Coarse-Resolution Ocean Models

Anand Gnanadesikan

Atmospheric and Oceanic Sciences Program, Princeton University, Princeton, New Jersey

Robert W. Hallberg

NOAA/Geophysical Fluid Dynamics Laboratory, Princeton, New Jersey

(Manuscript received December 8, 1997, in final form September 24, 1999)

DOI: 10.1175/1520-0485(2000)030<2013:OTROTC>2.0.CO;2

ABSTRACT

The response of the Circumpolar Current to changing winds has been the subject of much debate. To date most theories of the current have tried to predict the transport using various forms of momentum balance. This paper argues that it is also important to consider thermodynamic as well as dynamic balances. Within large-scale general circulation models, increasing eastward winds within the Southern Ocean drive a northward Ekman flux of light water, which in turn produces a deeper pycnocline and warmer deep water to the north of the Southern Ocean. This in turn results in much larger thermal wind shear across the Circumpolar Current, which, given relatively small near-bottom velocities, results in an increase in Antarctic Circumpolar Current (ACC) transport. The Ekman flux near the surface is closed by a deep return flow below the depths of the ridges. A simple model that illustrates this picture is presented in which the ACC depends most strongly on the winds at the northern and southern edges of the channel. The sensitivity of this result to the formulation of buoyancy forcing is illustrated using a second simple model. A number of global general circulation model runs are then presented with different wind stress patterns in the Southern Ocean. Within these runs, neither the mean wind stress in the latitudes of Drake Passage nor the wind stress curl at the northern edge of Drake Passage produces a prediction for the transport of the ACC. However, increasing the wind stress within the Southern Ocean does increase the ACC transport.

Table of Contents:
- Introduction
- Possible responses of
- The relationship between
- Response to Southern
- Conclusions
- REFERENCES
- TABLES
- FIGURES

1. Introduction

The dynamics determining the transport of the world's largest ocean current, the Antarctic Circumpolar Current (ACC), remain unclear. Toggweiler and Samuels (1993, 1995, 1998) and McDermott (1996) performed a number of sensitivity studies where they varied the magnitude of the wind stress south of 30°S in a large-scale general circulation model. They found that the magnitude of the current increased as the winds increased, as did the pycnocline depth to the north of the channel and the magnitude of the Northern Hemisphere overturning. The total amount of water upwelling through the equatorial pycnocline was inversely related to the magnitude of the wind stress in the Southern Ocean. Understanding what determines the ACC transport, how it has changed in the past, and how it could change in the future in response to changes in wind stress is thus of considerable importance.

This paper reviews three possible responses of the ACC in response to changes in the Southern Hemisphere winds.

1. The ACC transport could depend on the mean magnitude of the wind stress within the latitudes of Drake Passage, as proposed by Wang (1994), Wang and Huang (1995), Krupitsky et al. (1996), and others. In these models, changes in wind stress change the strength, but not the path of the ACC.

2. The ACC could be dependent on the wind stress curl at the northern edge of Drake Passage, as proposed by Stommel (1957), Baker (1982), and Warren et al. (1996, henceforth WLR). Changes in the wind stress that do not change the wind stress curl would not change the strength of the ACC.

3. The ACC could have very weak dependence on the wind stress. One way in which this could occur would be for the current to accelerate until lee waves formed by topography become stationary (Olbers and Völker 1996, Völker 1999). The mean speed of the current would then be determined by complicated nonlinear interactions between the lee wave and the mean current. Changes in the winds would change the path of the ACC near topography (changing the amplitude of the trapped wave), but would not necessarily produce large changes in the mean strength of the current. Straub (1993) also speculates that the ACC could accelerate until it became baroclinically unstable, at which point eddy transports would preclude development of further shear.

Although considerable work has gone into modeling the Circumpolar Current, little of it has been able to test the above hypotheses. The low-resolution simulations of Toggweiler and Samuels (1993, 1995, 1998) and McDermott (1996) are not of adequate resolution to properly test the final hypothesis, and cannot distinguish between the first two. High-resolution models have been used to make diagnostic calculations of the momentum balance (Stevens and Ivchenko 1997; Gille 1997), depth-averaged vorticity balance (Wells and DeCuevas 1995), and density balance (Saunders and Thompson 1993; Thompson 1993). However, these calculations suffer from the fact that the density structure is not in steady state (Killworth and Nanneh 1994), implications of which will be considered in more detail later in this paper. Additionally, the predicted strength of the current in both the FRAM and Semtner–Chervin models $O(180$ Sv) is considerably larger than the estimated 110–140 Sv (Sv $\equiv 10^6$ m^3 s^{-1}) from current meters (Whitworth et al. 1982; Whitworth 1983) and using hydrographic sections (Orsi et al. 1995). The results of these models have been used to attack the second hypothesis (Hughes 1997; Olbers 1998) even though multiple runs with different wind stress patterns were not done within the high-resolution models.

In general, work on what sets the transport of the Circumpolar Current has focused on the dynamic balances involved. This has some advantages in that the current comes into dynamic balance relatively quickly. The major point of this paper is that such an approach is insufficient for evaluating what sets the long-term mean transport. There is a strong meridional pressure gradient connected with the Circumpolar Current that cannot be determined from the Sverdrup balance or by looking at zonal pressure drops across ridges. We propose a mechanism by which the Circumpolar Current and density stucture of the rest of the ocean are connected as shown in Fig. 1. Northward transport of water in the Ekman layer drives a meridional overturning, with dense water being upwelled and lightened, initially by surface freshening in the Southern Ocean, but as the water moves farther to the north by warming as well. This light water is then injected into the pycnocline to the north of the ACC as Antarctic Intermediate Water and mode water.

Since light water is being added in the south, in order to maintain a steady state density field it must be taken out somewhere else. This primarily occurs in the North Atlantic as a result of Northern Hemisphere overturning. In the large-scale GCMs, the magnitude of the Northern Hemisphere overturning is directly correlated with the depth of the pycnocline (Bryan 1987; Park and Bryan 2000; Gnanadesikan 1999). Essentially, the density contrast between the high northern latitudes and the subtropical pycnocline produces a north–south pressure gradient. This pressure gradient in turn drives frictional currents along the boundaries (Bryan 1987; Hughes and Weaver 1994; McDermott 1996; Park and Bryan 2000;Gnanadesikan 1999). The deeper the pycnocline at low latitudes, the stronger these frictional currents and the water mass transformations that feed them become. It should be noted that this mechanism is exactly that used to drive meridional overturning in box models (Stommel 1961) and two-dimensional models of thermohaline overturning (Wright et al. 1998).

The response of the general circulation to changes in Southern Hemisphere winds can then be described as follows. If the winds in the Southern Ocean increase suddenly, more water will be added to the density classes in the lower part of the

pycnocline as a result of thermal damping. This means that more water is being added to these isopycnal layers than is being removed in the Northern Hemisphere so that the pycnocline must deepen. This deepening in turn causes an increase in Northern Hemisphere overturning with a concommitant increase in poleward heat transport and in the temperature of the deep waters formed in the Northern Hemisphere. Together, the deeper pycnocline and warmer northern deep waters result in an increase in the strength of the thermal wind shear within the ACC. Given that near-bottom velocities are relatively small (Whitworth 1983, for example found that the velocities at 2500 m could account only for one-fourth of the total transport), increasing the thermal wind shear increases the strength of the current. Eventually, the changes in density structure to the north of the ACC increase the Northern Hemisphere overturning until it balances the increased addition of light Southern Hemisphere water.

This paper has the following structure. Section 2 reviews the three possible responses to wind stress forcing in more detail, emphasizing that overlooking the effects of buoyancy forcing can have serious effects. Section 3 presents some simple numerical simulations that show how the interaction between buoyancy forcing and wind stress can affect the response of the ACC to winds. Section 4 considers a set of runs with an ocean general circulation model. Section 5 presents conclusions and suggestions for future work.

2. Possible responses of the Circumpolar Current to Southern Hemisphere winds

a. Dependence on the mean stress

The zonal momentum equation can be written

$$\frac{\partial u}{\partial t} + \frac{\partial}{\partial x}(uu) + \frac{\partial}{\partial y}(uv) + \frac{\partial}{\partial z}(uw) - fv = -\frac{1}{\rho}\frac{\partial p}{\partial x} + \frac{1}{\rho}\frac{\partial \tau_x}{\partial z}, \quad (1)$$

where τ_x is the frictional stress in the zonal direction associated with unresolved turbulence. If an average over depth and longitude is taken, it can be shown that at steady state the time-dependent term, the zonal momentum advection term, the vertical momentum advection term, and the zonal integral of the Coriolis term drop out (ignoring the Goldsborough circulation). Scaling arguments can be used to show that the meridional advection of zonal momentum is small, so the momentum balance becomes

$$\int_X \frac{1}{\rho}(\tau_x|_{z=0} - \tau_x|_{z=-D})\, dx = \int_X \int_{z=-D}^{0} \frac{1}{\rho}\frac{\partial p}{\partial x}\, dz\, dx. \quad (2)$$

The left-hand side represents the difference between the surface and bottom stresses. Since the latter are small (given relatively weak bottom velocities), it can be essentially replaced by the wind stress. The right-hand side of (2) represents the pressure difference across ridges, which is often referred to as the “form drag” or“mountain drag” in the oceanographic and meteorological literature (Munk and Palmen 1951). Since the deep flow is basically geostrophic, form drag is associated with a deep southward flow below the height of the ridges. Insofar as Eq. (2) holds, this deep geostrophic flow balances the northward Ekman flux associated with the wind stress. This is, in fact, the dominant balance in high-resolution general circulation models such as FRAM (Stevens and Ivchenko 1997) and the quarter-degree Semtner–Chervin model (Gille 1997) when a vertical integral is made.

Is this overturning linked to the strength of the ACC? Barotropic models can produce an effective overturning circulation when averaged along geopotential surfaces if northward flow occurs over ridge tops, southward flow occurs in troughs, and frictional boundary layers connect the two. This simple picture has been used by Wang (1994), Wang and Huang (1995), Krupitsky and Cane (1994), and Krupitsky et al. (1996) to argue that the ACC transport should scale as the wind stress. The basic assumption in all these models is that the paths of all the currents are fixed (presumably by the deep topography) and, thus, that the form drag scales as the strength of the current.

As will be shown below, this assumption is questionable in a stratified ocean. The key point is that the overturning circulation implied by the form drag balance in the absence of active eddies requires some buoyancy transformation not only in the Southern Hemisphere (to convert dense North Atlantic Deep Water into lighter Antarctic surface water, as noted by WLR) but also some compensating transformation of light water to dense water in the north. In large-scale ocean models this transformation is accomplished by a stronger overturning circulation driven by a deeper pycnocline and associated north–south pressure gradients. This deeper pycnocline, however, alters the meridional pressure gradient within the ACC,

thus changing the *path* of the current.

b. Dependence on the wind stress curl

An alternative suggestion has been present in the oceanographic literature for many years and has recently been taken up by WLR. It notes that the ACC is largely found at latitudes to the north of Drake Passage, and thus that Sverdrup theory should apply. The wind stress curl computed from the dataset of Hellermann and Rosenstein (1983) at latitudes just to the north of Drake Passage would support a southward transport of 130 Sv, tantalizingly close to the observed magnitude of the ACC. However, this wind stress field is not based on much data within the Southern Ocean. More recent wind stress products, for example the wind stress fields produced by the NCEP reanalysis project (Kalnay et al. 1996), have values of wind stress curl substantially larger (20%–30%) than the Hellermann–Rosenstein winds. It is thus possible that this agreement between wind stress curl and ACC transport argued by WLR is entirely fortuitous.

Several assumptions go into the argument that that ACC is determined by Sverdrup balance. In general, the vorticity balance in the oceanic interior is between vortex stretching and the advection of planetary vorticity,

$$\beta V_g = f(w_E - w_B), \quad (3)$$

where V_g is the meridional geostrophic transport at depths below the Ekman layer, w_E is the Ekman pumping, and w_B is the vertical velocity just above the bottom due to flows over topography. When Sverdrup balance holds, $w_B = 0$. Theories that assert the ACC transport is determined by the Sverdrup relation are effectively arguing that the effect of bottom velocities on vortex stretching is small. In that case, the meridional transport can then be integrated across the ocean interior to get a southward geostrophic interior transport, which is then balanced by a northward transport in the boundary current (though what constitutes the interior and what constitutes a boundary current may be controversial given the large number of deep topographic features that steer the Circumpolar Current). Continuity is then invoked to equate the northward boundary current transport along the coast of South America with the eastward transport in Drake Passage.

There has been little critical evaluation of the Sverdrup balance theory within the context of numerical models. Baker (1982) and Mestaz-Nunez et al. (1992) presented observational evidence that the dynamic topography of the ACC was qualitatively governed by the Sverdrup balance. However, Wells and DeCuevas (1995) argued that within FRAM, the classical Sverdrup balance was *not the dominant* balance when a circumpolar integration was made. Although they found that Sverdrup balance held over most of the Pacific and Indian Oceans, within the Atlantic sector topographic effects were extremely important. Essentially they found that water parcels that move south as tall columns in the ocean interior move north in the boundary current next to South America as short columns. It should be noted that this vorticity balance is just what would be expected from a form drag balance.

If the Sverdrupian theory were true, changing the mean wind stress within the Southern Hemisphere without changing the Ekman pumping would not change the meridional geostrophic flow within the ACC. If meridional pressure gradients or bottom velocities play a significant role in setting the current strength, the Sverdrupian theory will fail and the current can be sensitive to such changes in the wind stress field. This hypothesis is testable with numerical models.

c. Saturation of the ACC

A third suggestion has recently been proposed by Olbers and Völker (1997) and Völker (1999) based on the ideas of atmospheric blocking first explored by Charney and DeVore (1979). The basic idea is that the deep geostrophic flows are intimately connected to the surface geostrophic flows, but not in a linear manner as in the barotropic and equivalent barotropic work. The passage of the current over a ridge generates a lee wave. When the current becomes large enough to counter the westward propagation of baroclinic Rossby waves, the lee wave becomes trapped on the ridge and grows to large amplitude. Bottom friction acting on this lee wave generates a second lee wave out of phase with the ridge. This second lee wave has a pressure distribution that produces mean southward geostrophic flow below the ridge depth and mean northward geostrophic flow over the ridge, thus giving a form drag balance.

Such a picture of Circumpolar Current dynamics does not yield a simple dependence of ACC transport on wind stress. Larger wind stresses can result in lee waves with larger amplitude, but this can be accomplished by relatively small changes in the velocity, moving it closer to the resonance condition where the mean velocity is equal to the baroclinic wave speed. There is no buoyancy forcing in this description. The implicit assumption is that interfacial stresses (acting as a proxy for eddies) produce ageostrophic flows in the upper and lower layers that balance the mass fluxes associated with the Ekman and deep geostrophic flows respectively.

Similar ideas regarding transient eddies have been proposed by Straub (1993). The basic idea is that the northward export of light water associated with the Ekman transport causes the pycnocline to shoal in the Southern Ocean, creating a height

gradient in the dense layer underlying the pycnocline. In the absence of buoyancy forcing, this height gradient increases until the potential vorticity gradient in the lower layer is in the opposite direction from that in the upper layer. At this point, the current becomes baroclinically unstable, which results in the creation of mesoscale eddies. Balance is achieved when the mass fluxes associated with the eddies (which tend to smooth out the height gradients in the layers) counterbalance the Ekman and deep geostrophic mass fluxes. The current transport in this picture is controlled by the relative thicknesses of the fluid above and below the pycnocline (which determine at what point baroclinic instability sets in), but is insensitive to the magnitude of the surface stress.

The simulations presented in this paper are not sufficient to test these saturation hypotheses. Although coarse-resolution general circulation models do have a representation of stationary waves (the currents in the models do meander), that the horizontal resolution is so coarse may not allow for strong enough currents to build up over topographic features. Similarly, either multiple simulations that resolve the mesoscale eddy field under different wind stress fields or an accurate parameterization of the effects of these eddies is necessary to test the hypothesis of Straub (1993). Neither is available at the present time.

d. Problems with previous theories

The theories described above all assume that dynamic balances are sufficient to constrain the strength of the Circumpolar Current. It is far from clear that this should be the case. The reason is that the vertical shear within the Circumpolar Current is determined by the density field (Gill and Bryan 1971). It is important to consider what maintains this density field. Acting in isolation, the frictional surface flow and deep geostrophic flow acting alone would drain the Circumpolar ocean of light water and fill it with dense water. In order to counteract this one of two things must happen, as illustrated in Fig. 2 for an idealized two layer system.

One possibility (shown in Fig. 2a) is that the interface between the light water and dense water tilts, and the shear between the two layers builds up until it results in the upper layer exerting a stress on the lower one. This stress could be carried by standing eddies (as in Olbers and Völker 1997) or by transient eddies (as argued by Johnson and Bryden 1989 and Marshall et al. 1993). It should be emphasized that this picture does not imply that there is no Ekman layer in the Southern Ocean (contra Johnson and Bryden 1989, this point is also made by Olbers 1998). Form stresses associated with mesoscale eddies in continuously stratified models, for example, are small near the surface and bottom (where height displacements are small), but rise to large values within the interior of the water column (where height displacements are large). A steady state is reached when the stress between the upper and lower layer is equivalent to the surface wind stress (and cross-ridge pressure difference at the bottom). The result is that the mass transports implied by a deep geostrophic flow below the ridge depth and and Ekman transport in the surface layer are compensated by eddy-driven flows in both layers. The eddy stresses balance the surface stress and bottom pressure differences across ridges so that there is no net flow (and thus no net Coriolis force) within either layer (Olbers 1998). Within this picture the dynamics must play the dominant role in determining the response of the ACC to the winds since no thermodynamics are involved.

A second possibility involves exchange of fluid between the layers as the result of buoyancy forcing. Buoyancy forcing within the Antarctic has been traditionally thought of as driving two cells (Sverdrup et al. 1942). In one, the Circumpolar Deep Water is transformed to Antarctic surface water through cooling and freshening, and this freshwater is then warmed as it moves northward and is subducted at the Polar Front to form Antarctic Intermediate Water. In the other, the Antarctic surface water is enriched in salt through brine rejection, and mixes with Circumpolar Deep Water to form Antarctic Bottom Water. As pointed out by WLR, that the coefficient of thermal expansion is small at the surface means that over the Antarctic as a whole, the first cell will dominate the second, so there is a buoyancy transport of the right sign to connect the deep southward geostrophic flows with the northward Ekman flux. Because the buoyancy flux allows a net transport to occur in both the upper and lower layer, each layer can experience a net Coriolis force that can balance the surface wind and bottom pressure gradient without requiring interfacial stresses.

It is unclear which picture most resembles the real ocean, though both are probably operative. Results from the FRAM model, for example, support the idea that the first picture is dominant. Killworth and Nanneh (1994), show that in the FRAM model the vast majority of the 7 Sv of water lighter than $\sigma_0 < 27.5$ flowing northward at 56°S is supplied from water masses that neither touch the surface nor the bottom. However, because in the FRAM model many of the deep isopycnal layers are filling or emptying, it is unclear where these waters that feed the Antarctic surface water actually originated, and thus whether changes in Southern Hemisphere winds would be compensated by changes in the local gyres and transient eddies or by pycnocline deepening and greater Northern Hemisphere overturning. Conversely, Warren (1990) argued that the geostrophic flow at intermediate layers that intersected neither the surface nor the bottom would have to be zero when integrated around the entire Southern Ocean. This would seem to imply that the northward Ekman flux would have to be closed by transforming deep flows that intersect topography. Since the density classes that occur at such depths are of polar origins, this would favor the second picture.

Whether one picture is dominant in a particular numerical model depends on exactly how the buoyancy fluxes are applied.

If there are no buoyancy fluxes at all, dynamic balances must come into play to bring about a steady-state density field, as in Fig. 2a. If the buoyancy flux is in some way dependent on the density field, so that more light water in northern latitudes results in a stronger cooling at those latitudes, then the relationship between ACC transport and wind can be closely related to the buoyancy flux. In the following two sections, we present two systems where the thermodynamics are very important. In both of them, Sverdrup balance governs the interior flow and form drag describes the vertically and zonally averaged momentum balance. However, neither Sverdrup balance nor form drag correctly predicts the dependence of the ACC transport on the winds. Changes in the transport through an open passage can be produced without changing the wind stress curl to the north of the passage, contradicting the hypothesis the Sverdrup balance is predictive. Additionally, in contrast to the linear models of Wang (1994) and Krupitsky et al. (1996) the models with thermodynamic forcing do not produce a simple linear relationship between form drag and current transport, so form drag does not provide a predictive theory for the transport of the current. Although these models are not good tests of the saturation hypothesis, they should be good tests of the other two hypotheses for how the transport of the Circumpolar Current is set.

3. The relationship between buoyancy forcing and dependence on the wind stress: Simple model experiments

a. Model setup

Figure 3 shows a simple scenario used here to consider the effect of wind stress and buoyancy forcing on the Circumpolar Current. Model runs were made using the isopycnal coordinate model of Hallberg (1995). A reentrant basin 100° latitude by 50° longitude was used. The basin geometry is shown in Fig. 3a. The basin is reentrant with a silled channel between 0 and 10°E. The sill has a depth of 2000 m. The interior basin has a flat bottom with a depth of 4000 m. The model has two layers, an upper layer 1500 m thick and a lower layer 2500 m thick. All geostrophic contours are blocked in the lower layer, but there are unblocked geostrophic contours within the upper layer. Wind stress forcing is applied over the 10 degree strip shown by the shaded patch. Four wind stress fields were used. The base case produces no Ekman pumping except far to the north and south of the channel latitudes, as shown in Figs. 3b,c. The other three runs added a Gaussian jet of winds with a half width of 5 degrees centered on the northern edge of the passage, the center of the passage, and the southern edge of the passage. These three cases are referred to as the northern jet, centered jet and southern jet, respectively. The model resolution was 0.75° in the zonal direction and 0.5° in the meridional direction. A horizontal viscosity of 2×10^4 m^2 s^{-1} was used.

b. Buoyancy flux closed by interface restoring

In order to explore the question of how buoyancy flux could determine the response of the ACC to winds, a series of runs was made in which the buoyancy flux was parameterized by damping the interface between the layers back toward its initial value. This results in a diapycnal velocity w,

$$w = -\lambda(h - h_0), \quad (4)$$

where λ is a damping coefficient, h is the height of the interface between the two layers, and h_0 is the unperturbed height of the interface. Kawase (1987) used a similar closure for buoyancy forcing in looking at the response of the deep stratification to changes in dense water production. This forcing produces a lightening of the deep water when the interface is displaced upward and an increase of the density of the light water when the interface is displaced downward. It therefore leads to a flow of water from the dense to the light layer in the southern part of the basin, where light water is being exported northward, and a flow of water from the light to the dense layer in the northern part of the basin. These buoyancy fluxes close the circulation associated with the Ekman flux. A circulation where water becomes lighter within the Southern Ocean is consistent with the argument of WLR, although no claim is made here that the way in which the forcing is implemented is realistic.

This parametrization of buoyancy forcing implies that the mean interface height displacement to the south of the channel gives the total buoyancy forcing to the south:

$$\langle Q \rangle_s = \lambda(\langle h \rangle_s - h_0)\delta\rho, \quad (5)$$

where $\langle\ \rangle_s$ denotes averaging over latitudes to the south of the channel. At steady state

$$\langle Q \rangle_s A_s = F^{\mathrm{Ek}}{}_s \delta\rho = \lambda(\langle h \rangle_s - h_0) A_s \delta\rho \quad (6)$$

so that

$$\langle h \rangle_s - h_0 = F^{\mathrm{Ek}}{}_s / A_s \lambda, \quad (7)$$

where A_s is the area of the basin to the south of the passage and $F^{Ek}{}_s$ is the Ekman flux at the southern edge of the channel. Thus the interface height rise to the south of the channel is directly related to the export of water from the southern part of the basin. Similarly, the interface height drop to the north of the channel is linearly related to the import of light surface water:

$$\langle h \rangle_n - h_0 = -F^{Ek}{}_n / A_n \lambda. \quad (8)$$

Defining the shear transport $T^{shear}{}_{ACC}$ as the zonal transport due to the geostrophic shear between the upper and lower layers,

$$T^{shear}_{ACC} = (u_1 - u_2)H_1 = \frac{g(\langle h \rangle_n - \langle h \rangle_s)H_1 \delta\rho}{\rho f}$$

$$= \frac{gH_1 \delta\rho}{\rho f}\left(\frac{F^{Ek}_n}{A_n \lambda} + \frac{F^{Ek}_s}{A_s \lambda}\right), \quad (9)$$

where $u_{1,2}$ are the velocities in the upper and lower layers respectively, g is gravity, $\delta\rho$ is the difference in density between the two layers, ρ is a mean density, and H_1 is the thickness of the upper layer. The total transport is then the shear transport plus a deep transport $T^{deep}{}_{ACC}$, which corresponds to the zonal velocity in the deep layer integrated over the depth of the water column.

The model was initially run with $\lambda = 0.001$ day^{-1} and $g\delta\rho/\rho = 0.019$ m s^{-2}. Together with areas for the southern and northern basins of 1.8×10^{12} m^2 and 3.8×10^{13} m^2, respectively, a baseline Ekman flux of 0.75 Sv, and taking f at the middle of the channel, this produces an estimated $T^{shear}{}_{ACC}$ of 8.5 Sv. Figure 4a shows the actual solution, which has a total transport of 10.4 Sv and a shear transport of 9.6 Sv. The agreement is suprisingly good considering the numerous physics that have been neglected (friction, the fact that the height anomaly, shown in Fig. 4b need not be uniform throughout the basin, etc.). The meridional flow patterns away from the circumpolar region are easily comprehensible (Fig. 4c,d). In the upper layer, there is northward flow over the band of longitude where there is wind stress, with weak modification by Munk boundary layers. On the western boundary, some portion of the flow is returned in the upper layer and some portion in the lower layer, with the balance shifting from the upper to lower layer as one moves from north to south.

The mean height difference across the interior basin is shown in Fig. 5a for the baseline case. To the north of the channel, there is a weak depression of the pycnocline by an average of 1.79 m [compared with 1.73 m predicted from (8)]. To the south of the channel the pycnocline rises by 30.3 m, [compared with 35.9 m from (7)]. As the wind field is changed by adding a localized jet (Figs. 5b–d), the changes in the interface height do track the predictions, showing the largest height difference for the southern jet, with successive decreases in the height difference and current strength as the jet is moved northward. However the details of the height field change so that in some cases there appears to be one coherent Circumpolar Current, while in others there are clearly two currents. The resulting transports are shown in Table 1.

The velocity fields for all four runs with interface damping are shown in Fig. 6. The addition of wind stress curl does produce a counterclockwise gyre to the north of the jet with a clockwise gyre to the south. The effect is to shift the central latitude of the ACC. Notice that the northern jet case is qualitatively similar in structure to the real ACC, with the bulk of the current to the north of the channel. This is because the westward drift associated with the gyre circulation to the south of the wind stress jet counters the eastward drift produced by the mean meridional pressure gradient associated with the export of light water from the Antarctic.

The dependence of the ACC on wind stress is quite compatible with the theory developed earlier in this section. Equation (9) gives a good prediction of the ACC transport, indicating that it should increase for all three wind jets, but that by far the largest increase should be for the jet centered at the southern boundary. This is in fact the case.

By contrast, it is difficult to understand the changes in transport within the passage in terms of the changes in the mean wind stress. The centered jet case has a lower transport than the southern jet case, even though the wind stress within the latitudes of the passage is higher for the centered jet. This is despite that the depth-integrated momentum balance within the channel is largely between pressure differences below 2000 m and wind stress (Fig. 7) in all four runs. That this form

drag balance holds does not translate into a current dependent on the mean strength of the winds within the passage since the path of the current (as seen in Fig. 6) is not fixed.

Similarly, it is difficult to understand the response of the modeled Circumpolar Current to wind stress in terms of changes in the Ekman pumping. Relative to the baseline case, for example, the northern jet has slightly more transport even though the Ekman suction to the north has decreased. The model response is opposite to that predicted by the Sverdrupian theory. This is despite the fact that the spatial structure of the meridional flow can be entirely understood in terms of Sverdrup dynamics with Munk boundary layers. As in the case of the form drag balance, Sverdrup balance provides a prediction of the meridional, but not the zonal, flows.

c. Buoyancy circulation closed with fixed sources and sinks

An interesting contrast to the above results is found when the buoyancy flux associated with the overturning is closed by fixed sources and sinks of fluid. A model run was made in which the Ekman transport was balanced by a flow from the heavy layer to the light layer centered at 70°S, 15°E and a flow from the light layer to the heavy layer centered at 20°N, 15°E. As shown in Fig. 8, there is now essentially no Circumpolar Current associated with the Ekman transport, despite that the southward geostrophic flow below the sill depth balances the northward flow in the Ekman layer (Figs. 8c,d). The meridional flows are qualitatively very similar to those with interfacial damping, and the force balance (not shown) is essentially the same.

This case illustrates the statement of WLR that the form drag balance, by itself, tells us nothing about the transport of the ACC. When there is buoyancy forcing the applicability of bottom form drag does not imply the existence of interfacial form drag or internal vertical viscous stresses. For the case in Fig. 8, the existence of deep geostrophic flows does prevent the ACC from accelerating. This is not because the associated interface displacements cause a “stress” between the upper and lower layers, decelerating the upper layer and accelerating the lower layer. The upper layer momentum balance is simply that of an Ekman layer, where the wind stress and Coriolis acceleration balance. Instead, the deep geostrophic flows feed diapyncal mass fluxes that prevent the internal interface from being displaced upward in the south and downward in the north. This in turn prevents the development of a meridional pressure gradient that would drive a Circumpolar Current.

Despite many unrealistic features, this simple model demonstrates that the wind-driven response of a reentrant basin can depend critically on how dense water is transformed into light water, and vice versa. This is in contrast to closed basins in which density transformation does not change the Sverdrup circulation at all. The difference arises because a reentrant domain allows for the presence of a mean zonal flow driven by a meridional pressure gradient. As long as the channel is much larger than the baroclinic radius of deformation, such a pressure gradient will be sustainable. In the present model this pressure gradient is directly linked to the strength of the Ekman transport at the northern and southern edges of the channel.

The model illustrates the fundamental difference between the ACC and other parts of the World Ocean. When there are blocked geostrophic contours in both warm and cold water spheres, a change in the mean Ekman flux can be balanced by a southward geostrophic transport within the surface layer, with no density transformations necessarily implied. However, because of the open upper layer geostophic contours within Drake Passage, this is not true for the ACC. Northward flow in the surface layer must be balanced by deep geostrophic flow below the ridge depth. Unless the isopycnal displacements are very large, this implies density transformation or strong eddy fluxes.

d. The deep flow and its dependencies

The previous subsections have focused on the vertical shear. In order to understand how the total transport is determined, it is also important to understand what sets the deep transport. It is clear from inspection of Table 1 that a simple dependence on the wind stress curl north of Drake Passage does not account for the deep transport (since this would predict no increase for the southern jet and a decrease in the transport for the northern jet). There also appears to be a scaling between the shear and deep transports, with the latter being about 10% of the former. Explaining why this is the case, however, turns out to be a daunting problem since the actual value of the deep flow turns out to be extremely sensitive to the details of topography, stratification, and friction. This is illustrated in Table 2, which shows how the shear and deep transports are changed by changes in the model setup.

The first two runs reported in Table 2 demonstrate that the deep flow is quite sensitive to the details of the topography. Both runs were made with the topography within the channel changed from a simple plateau 2000 m high to a north–south ridge 2000 m high. While the shear transport changed relatively little in these cases (10%–15%), the deep geostrophic transport changed by a factor >3. It should be pointed out that, were the Sverdrupian explanation favored by WLR to be operating here (and there is no reason why it should not), changing the topography within the channel should have no effect on the transport at all.

The third run reported in Table 2 demonstrates that the deep flow is more sensitive to friction than the shear flow. Doubling the frictional coefficient reduces the shear flow by only 15% (comparing the first and third lines of Table 2), while it reduces the deep flow by more than 30%. This indicates, incidentally, that the shear flow is only weakly affected by friction. Again, such a change in the deep flow would not be expected were the Sverdrupian explanation of ACC transport to describe this situation.

The final run reported in Table 2 demonstrates that the deep flow depends on the stratification. In this run the depth of the upper layer is reduced from 1500 to 1000 m. From Eq. (9) this would be expected to result in a decrease in the shear transport by one third. The actual change is close to this (39%). The deep transport, by contrast increases by a factor of 2.

That the deep transport is so sensitive to details of the topography, friction, and stratification is not surprising. As noted by Hallberg (1997) in the presence of finite amplitude topography, the large-scale planatary wave that establish the structure of the flow experience scattering. The details of the scattering, however, depend on the details of the stratification and topography and the structure of the currents established depends on the friction. This means that it is unlikely for a simple theory to be able to describe the relationship between the deep transport and the shear transport.

e. Conclusions that can be drawn from the simple model

Several lessons emerge from the simple models presented in this section.

1. Buoyancy forcing can determine how the wind stress produces a meridional pressure gradient across latitudes where there is an open passage. Some patterns of buoyancy forcing (as in section 3c) can counteract the tendency of the Ekman transport to produce any meridional pressure gradient, while others (as in section 3b) do not.

2. As a result, the same wind stress forcing can produce many different ACC transports, depending on the buoyancy forcing. These different currents may all involve a “form drag” type of balance when the momentum equations are vertically integrated.

3. The fact that away from the channel vorticity dynamics are given by Sverdrup balance with Munk boundary layers does not imply that Sverdrup balance predicts the flow through the channel.

4. In all of the model runs presented here, there is a relationship between the shear transport and the deep transport. However the details of this relationship are dependent on details of the topography, friction and stratification. Because of this, it seems unlikely to us that a general theory which describes the deep flow will be quickly forthcoming.

4. Response to Southern Hemisphere winds in a GCM

a. Model setup

In order to look at a more realistic scenario, a number of runs were made with the Modular Ocean Model (Pacanowski 1996). These runs span the entire globe at a resolution of 3.75° in the meridional direction and 4.5° in the zonal direction. Surface salinity and temperature were restored to the Levitus dataset. Vertical mixing is given by the parameterization of Bryan and Lewis (1979) that uses a value of 0.3 $cm^2\ s^{-1}$ in pycnocline and 1.3 $cm^2\ s^{-1}$ in the abyss with a transition at 2500 m. Mesoscale eddies are assumed to mix in the horizontal only. All cases were run out for 2000 years at which time they are essentially in equilibrium.

The response of this model to changes in the magnitude (but not the pattern) of the wind stress field was studied by Toggweiler and Samuels (1993, 1995, 1998) and McDermott (1996). They found that increasing the wind stress field increased the transport of the Circumpolar Current, the overturning circulation, and the depth of the pycnocline. The Circumpolar Current transport was found to increase linearly with the wind stress field. Gnanadesikan (1999) also analyzed a similar model in which the vertical transport of momentum (and horizontal transport of mass) due to mesoscale eddies was included. These runs also produced a linear relationship between the ACC transport and wind stress. Since the pattern of wind stress was not changed, however, these runs do not provide a test for whether certain specific latitudes are especially important (the wind stresses at all latitudes scale together) or whether Sverdrup balance is predictive (the wind stress curl increases as the wind stress does).

In order to look at the response of the model to Southern Hemisphere winds in a more general way, offsets in the winds similar to those imposed in the idealized runs were applied. A summary of the different runs is given below.

1. The baseline run (BA) uses winds given by Hellerman and Rosenstein (1983).

2. Three cases were run with winds south of 30°S multiplied by a constant, paralleling those of Toggweiler and Samuels (1995) and McDermott (1996). Zonal winds south of 30°S (the latitude of zero mean zonal wind stress) were scaled by 0, 50%, 150%. These runs do not provide a means for distinguishing between different mechanisms for explaining the transport of the ACC, but they do provide a means for evaluating the linearity of the solution, and the contribution of buoyancy forcing. The three runs are referred to as no winds (NW), reduced winds (RE), and increased winds (IN).

3. Parallel to the previous section, wind stress field perturbations were added to the Hellerman and Rosenstein winds. Two such perturbations were added in which the wind stress depended on the tangent of the latitude θ:

$$\Delta\tau^x = \tau_p \tan(\theta), \qquad \theta < 0. \tag{10}$$

This perturbation wind stress field does not change the Ekman pumping on a sphere except at the ocean boundary. Two values of τ_p were used, one corresponding to an increase in the Ekman transport [positive offset (POF)] and another corresponding to a decrease in the Ekman transport [negative offset (NOF)]. Since these cases have identical Ekman pumping within Drake Passage, a Sverdrupian scaling for the ACC would predict that they would have an identical ACC transport as the baseline case. The theories that suppose the ACC to scale with the average winds would predict an increase for the positive offset and a decrease for the negative offset.

4. Several cases were run where the perturbation added to the baseline Hellerman–Rosenstein winds was a zonal jet of winds, again paralleling the simple model results of section 3a. For these cases the perturbation was

$$\Delta\tau^x = 0.5 \cos[(\theta - \theta_0)/\Delta\theta], \ \theta_0 + \Delta\theta > \theta > \theta_0 - \Delta\theta, \tag{11}$$

where $\Delta\theta$ was the channel width. Four values of θ_0 were run, with the additional jet of wind centered at the northern edge of the passage (NJ), centered within the passage (CJ), at the southern edge of the passage (SJ), and to the south of the passage (FSJ), paralleling the runs discussed in section 3.

b. Model results

The GCM predicts a complicated relationship between the wind stress field and the ACC transport. A summary of the how different wind stress fields alter the mean wind stress within the channel, wind stress curl to the north of the channel, wind stress at the southern edge of the channel and ACC transport (relative to the baseline case) is presented in Table 3. The key is that as the wind stress within the channel increases; so does the ACC transport. Such a simple relationship does not hold for the Ekman suction at 51.1°S since the ACC transport can increase even when the Ekman suction decreases. This leads us to believe that Sverdrup balance does not predict the ACC transport.

This conclusion holds when a more quantitative evaluation is made. A full tabulation of the numerical model results is presented in Table 4, and the ACC transport is plotted against the wind stress in Fig. 9a. Although the data in Table 4 and Fig. 9a show some relationship between the average wind stress in the channel and the ACC transport, the relationship is not simple. The reduced wind stress case (RE) has a much larger average stress in the channel than the negative offset case (NOF), yet the transports are quite close. There is an enhanced response to winds at the northern edge of the channel. This can be seen by considering the cases where a jet of winds is added to the forcing fields. The northern jet case produces the strongest response relative to the baseline case, increasing the transport by 24 Sv, with the centered jet (+17 Sv), southern jet (+13 Sv), and far southern jet (+7 Sv) producing weaker responses. This is despite the fact the centered jet has the same wind stress, averaged over the channel, as the northern jet.

By contrast, the ACC transport is not related to the wind stress curl at 51.1°S (Fig. 9b). The northern jet (NJ) and centered jet (CJ) cases have a wind stress curl of the opposite sign as the baseline case, yet have a larger ACC transport. The southern jet (SJ) and far southern jet (FSJ) cases have the same wind stress curl at the north, but also show increases in total transport. The correlation coefficient between the wind stress curl and transport is small (0.25) and drops to −0.04 when the case without winds (NW) is omitted. For this model, at least, there is no discernable relationship between the wind stress curl and ACC transport.

The question of how much of the modeled changes in transport is due to changes in the thermal wind shear and how much is due to changes in the deep flow is not an easy one to answer. This is in part because changes in the deep flow in one location can become magnified in their effect over topography (as discussed by Hallberg 1997). A small eastward geostrophic flow in a deep layer may become much larger as it squeezes over a topographic bump. Over topography the effect of the “constant of integration” represented by the deep meridional pressure gradients may be much more important. Given the rough topography of the Southern Ocean, there is no single point at which the deep flows may be defined unambiguously. Figure 10 shows the deep transport (defined as the transport due to the velocities at the lowest grid point

integrated over the entire water column) at two points. One (at 67.5°W) is within Drake Passage, the other (at 52.5°W) lies to the east. Within the channel, the deep transport are a considerable percentage of the total transport, ranging from 25% to 60%. Downstream of the channel the values are much smaller, ranging from −17% to 24%. The deep transports also are related to the average winds within the channel latitudes. They do not appear to have any relationship with the wind stress curl (Figs. 10c,d).

It should be noted that the deep transports within the channel and upstream of the channel have different dependencies on wind stress. The IN and POF cases, for example, have essentially identical deep transports within the channel (159 Sv) but very different deep transports to the east (38 and 64 Sv respectively). The response of the deep transports to the east appears to be nonlinear as well so that the RE, BA, and IN cases do not lie on a straight line as they do within the channel.

A more detailed picture of the ACC in different runs illustrates the failure of either the mean stress or the wind stress curl to predict the ACC transport. Figure 11 shows the results from four runs. In the absence of any winds (Fig. 11a), there is still a reasonably strong ACC with a transport of about 80 Sv. Given that the pycnocline is too deep in this model, this result is probably erroneous. Runs made with weaker vertical diffusivity and a parameterization of mesoscale eddies have been found to yield weaker values for the ACC and thinner, more realistic, pycnoclines (Danabasoglu and McWilliams 1995; Gnanadesikan 1999). The addition of the baseline winds (Fig. 11b) produces a strong addition to the ACC of about 120 Sv. When the reduced winds (case RE) are applied, this wind-driven component is smaller but has a very similar structure (Fig. 11c). Runs similar to these were reported in Toggweiler and Samuels (1995). They do not distinguish between whether the ACC responds to the wind stress or to the wind stress curl since both decrease. The negative offset (NOF) wind stress case (Fig. 11d), however, has a smaller mean wind stress within Drake Passage than either the baseline or reduced winds case, but with an Ekman pumping identical to the baseline case. The result is a streamfunction field that looks very similar to the reduced wind stress case.

However, that two streamfunction fields look similar does not mean that the momentum balance is identical. The momentum balance within Drake Passage for the three cases with winds for the BA, RE, and NOF cases is shown in Table 5. For both the RE and BA cases, form drag is the dominant balance, with deep cross-ridge pressure gradients taking up almost 80% of the surface wind stress and meridional diffusion taking up most of the rest. For the NOF case, even though the transport is close to the RE case, the path of the current is different and the effect of diffusion is much more important, especially at depth.

c. What causes the model to be sensitive to the wind stress?

Why are there differences between the baseline and offset cases? This question is considered by focusing on the vorticity balance in the southeast Pacific, where the bottom in this model is relatively flat. Figure 12a shows the profile of the mean zonal velocities in the southeast Pacific along 57.8°S for the baseline and negative offset cases. The zonal velocities are much smaller in the negative offset case throughout the water column. In both cases the velocities are small at depth so that the decrease in the NOF case arises from a decrease in the thermal wind shear. These large changes in the thermal wind shear are not associated with large changes in the vertical velocity (Fig. 12b), which is very similar over the top part of the water column for both cases. In fact, near the surface the vertical velocity is identical since the Ekman pumping is the same in both model runs. The only differences arise at depth, where changes in the thermohaline circulation produce changes in the deep vertical velocities. The interior of the water column largely follows the geostrophic vorticity relation, as can be seen from Figs. 12c and 12d, which show the transport between 50 and 1895 m and the associated transport due to vortex stretching $(f/\beta)\partial w/\partial z$. In both the baseline and negative offset cases, these two terms roughly balance, so (3) is approximately satisfied. On small scales, structure in the vertical velocities is partially balanced by friction, but the large-scale balance is largely a geostrophic vorticity balance. There are some changes between the two cases due to changes in the deep vertical velocities, however, so that the classic *wind-driven* Sverdrup balance is not maintained, and the two transports are slightly different.

Despite changes in detail, however, the meridional transports are far more similar than the zonal transports for the negative offset and baseline case. This is because, as in the simple models, decreasing the wind stress changes the structure of the pycnocline, causing it to shoal to the north of Drake Passage and also decreasing the density slightly to the south of the passage. Figure 13 illustrates how these changes occur, showing that the σ_0 = 27.4 isopycnal shoals by almost 500 m to the north of Drake Passage relative to the baseline case when the negative offset is applied. In general, there is a slight decrease in the densities to the south of the passage when the negative offset is applied, but a large increase in the pycnocline densities to the north of the passage. The response of the density field to changes in wind stress is clearly global in extent (Fig. 13d) with the largest changes being seen at middepth. McDermott (1996) found similar changes in response to changing Southern Hemisphere winds.

These changes can have a significant effect on the total transport through the passage. Assuming that thermal wind shear holds, that flows right at the bottom are small, and that U is an average velocity at some height D above the bottom

$$U \approx \frac{g\delta\rho}{\rho f L} D, \qquad (12)$$

where $\delta\rho$ is the density difference across the passage, L is the width of the passage, and f is a scale value for the Coriolis parameter. If this is integrated over width of the passage and the remaining depth of the water column $H - D$ (H the total depth), then the effect of the deep density gradient on the transport above the sill depth M is

$$M \approx UL(H - D) \approx \frac{g\delta\rho}{\rho f} D(H - D). \qquad (13)$$

A representative magnitude of the effect of the deep changes in density (below 2500 m) can then be found by setting $\delta\rho$ = 0.04 kg m^{-3}, D = 3000 m, and H = 5500 m The resulting change in the transport is 30 Sv. A similar calculation shows that the effect of the density changes shallower than 2500 m could easily be 30–40 Sv, so about half of the change in transport between the BA and NOF cases can be explained by a decrease in the deep density gradient and the other half by a decrease in the density gradient at mid-depths.

d. Southern Ocean winds and Northern Hemisphere densities

In order to understand why changing the winds in the Southern Ocean should result in the density changes seen in Fig. 13, it is necessary first to divide the problem into two parts. The first is to understand why the pycnocline becomes shallower when the Southern Ocean winds weaken. The second is to understand why there is a concommitant change in the deep density gradient. We attempt to answer both questions within the framework developed in Gnanadesikan (1999).

This framework proposes that dense water is converted to light water within the Southern Ocean, first by freshening and then by warming as it moves northward in the Ekman layer. The rate at which this light water is created and transported northward goes as the Ekman transport and is thus proportional to the wind stress. This is indeed the case in the GCM (Fig. 14a) with changes in the northward transport of light water being of comparable magnitude to changes in the Ekman transport. As noted in section 2, this means that the momentum balance within this light fluid cannot be simply between wind stress and interfacial form drag, as in Fig. 2a, since there is a net Coriolis force on the light water. Rather, there must be a considerable diapycnal flux as in Fig. 2b.

In order for the density field to come to steady state, changes in the rate at which light water is formed in the south must be balanced by changes in the rate at which dense water is formed in the north. This means that the magnitude of the Northern Hemisphere overturning must change. In coarse-resolution models, the strength of the Northern Hemisphere overturning is linked to changes in the meridional pressure gradient (Bryan 1987; Hughes and Weaver 1994; Park and Bryan 2000). In models where the surface heat and moisture fluxes are parameterized by restoring the near-surface temperature and salinity to observations, the primary means by which the pressure gradient changes is by changing the depth of the pycnocline (Park and Bryan 2000). Thus a smaller Ekman flux in the Southern Ocean requires a smaller Northern Hemisphere overturning which in turn requires a shallower pycnocline (Fig. 14b;see also Gnanadesikan 1999). The northward heat transport in the Northern Hemisphere is simply correlated to the strength of the overturning (Fig. 14c).

The response of the pycnocline in the GCM is analogous to the simple model with interface restoring of section 3a. As the Ekman flux to the north increases, the pycnocline depth increases as well in order to drive a larger flux from the light layer to the dense layer. Unlike the simple model however, the restoring times for the basin to the north of the sill and that to the south are not equal. The restoring rate to the south is large, as there is a lot of vertical exchange and convection in this model. Thus the average pycnocline depth to the south of Drake Passage does not respond strongly to changes in the Ekman flux. By contrast, the restoring rate to the north (the effective λ) is very small, so changes in the Ekman flux and thus in the buoyancy transport can produce large changes in the interface height, which then feed back to give a stronger Circumpolar Current (as schematically shown in Fig. 1).

The changes in northward heat transport have an important effect on deep temperatures. As less heat is deposited in the North Atlantic by the circulation, less heat must be removed by surface fluxes. Since the model produces heat fluxes by restoring surface temperatures towards observations, lower heat fluxes require a smaller difference between modeled and observed temperatures, resulting in a cooler surface. The regions where this occurs include those areas where deep water is formed in the model. As a result, deep temperatures to the north of the Circumpolar Current (which are strongly affected by Northern Hemisphere deep-water formation) are strongly correlated with northward heat transport in the Northern Hemisphere (Fig. 14d). Changes in the temperatures to the south of the Circumpolar Current, by contrast, are relatively small. Thus, decreasing the winds in the Southern Ocean decreases the deep thermal wind shear and reduces the Circumpolar Current transport.

In summary, this section has argued the following.

1. In an ocean general circulation model with restoring surface conditions, the baroclinic part of the Circumpolar Current depends directly on the winds within Drake Passage.

2. This is because the winds within the passage determine to a large extent the amount of dense Circumpolar Deep Water that must be converted to lighter intermediate and mode waters.

3. Increasing the formation rate of these light waters causes the pycnocline to deepen until such point as the overturning in the Northern Hemisphere strengthens so that an equivalent amount of light water is converted back to dense water. This produces an increase in the north–south density gradient above the sill depth.

4. The increased overturning circulation increases the heat transport between the Southern and Northern Hemispheres, which cools the Southern Ocean and warms the Northern Ocean. These changes are then reflected in the north–south density gradient below the sill depth.

5. The changes in north–south density gradient produce a stronger current.

6. The meridional pressure gradient can change even if the zonal pressure gradients, which in the interior are determined by geostrophic vorticity balance, do not change.

5. Conclusions

This paper has argued that the relationship of the Circumpolar Current to Southern Hemisphere winds on long timescales is determined by thermodynamics as well as dynamics. The thermodynamic balance of the global ocean is quite sensitive to the strength of the winds in the Drake Passage latitudes. Increasing the winds in these latitudes increases the transformation of dense water to light water within the Southern Ocean, which must be compensated by a stronger Northern Hemisphere overturning. A deeper pycnocline and warmer bottom waters to the north of the ACC are associated with the stronger overturning.

The changes in meridional density gradients result in changes in the vertical shear of the zonal velocity within the ACC. The result is that the path of the ACC can change so that overly simple arguments based on some linear relationship between form drag and the ACC transport will not hold. Additionally, dynamical arguments based on Sverdrup balance will not work either. There is no evidence in our models that the ACC transport is related to the wind stress curl.

Although there are many limitations to the results presented in this paper, preliminary model runs indicate that some of the most obvious may not be extremely important. For example, in the OGCM the surface densities are set by a restoring condition—which might “set” the path of the current. In order to test whether this is really important, preliminary experiments have been made with an ocean general circulation model coupled to an atmospheric energy balance model without a hydrological cycle. In this model the incoming solar radiation is set and the sea-surface temperatures are allowed to vary. For several highly idealized runs, the basic mechanism outlined in this paper has been found to hold. More realistic runs with a hydrological cycle are currently being carried out.

A second limitation of this paper is the overly simple handling of the effects of mesoscale eddies. Such eddies can play a significant role in the momentum and mass balance within the Southern Ocean (Saunders and Thompson 1993). As illustrated in Fig. 2, insofar as eddies create interfacial stresses between the warm water and cold water spheres, they can counteract some of the necessity for density transformation. This effect was not included in the models presented in this paper. Moreover, it is increasingly clear that the dominant diffusive effect of the eddies is to mix along isopycnal surfaces rather than horizontally, as was done for the model runs in this paper. This means that the effective diapycnal diffusivity in these models is probably too large. Gnanadesikan (1999) shows that the effect of neglecting eddy momentum fluxes is to overestimate the degree to which Southern Hemisphere waters feed the Northern Hemisphere overturning, while overestimating the diapycnal diffusivity has the opposite effect. The basic insensitivity of the ACC transport to wind stress curl is probably not affected by these inaccuracies, as it has also been found in a model with a smaller diapycnal diffusivity and a parameterization of eddy momentum fluxes (Gent et al. 2000).

It is possible, however, that the failure of the coarse models to actually resolve eddies may lead them to ignore the possibility that the Circumpolar Current is actually saturated with respect to the winds. The only way to test this hypothesis is to run eddy-resolving calculations with different wind stress fields. We are beginning to investigate this question using a variety of models. Preliminary results with a two-layer model indicate that, when the current is baroclinically unstable throughout its course, increases in wind stresses result in more energetic eddies and larger eddy transports. However, eddy activity in the real Circumpolar Current appears to be concentrated downstream of topographic disturbances (Gille and Kelly 1996), so it is unclear to what extent these idealized results apply to the real ocean. Over the past year, a group of

investigators at the Geophysical Fluid Dynamics Laboratory has begun to develop a hierarchy of high-resolution general circulation models to attack this question.

The dependence of ACC transport on the thermodynamics is a somewhat unpleasant fact. It implies that the problems of understanding the density structure to the north of the Southern Ocean and understanding the thermodynamic balances within the Southern Ocean cannot be separated. Moreover, although simple balances that try to relate the ACC to the wind stress or wind stress curl may have some predictive skill on short timescales, they will fail to capture the true processes that set the meridional pressure gradient on long timescales.

Acknowledgments

AG was supported under the GFDL Visiting Scientist Program and by the Carbon Modelling Consortium, NOAA Grant NA56GP0439. RWH was supported by the Geophysical Fluid Dynamics Laboratory and by a UCAR Fellowship. The authors thank Isaac Held, Robbie Toggweiler, Young-Gyu Park, Steve Griffies, Christoph Völker, Dirk Olbers, and Bruce Warren for useful discussions.

REFERENCES

Baker, D. J., 1982: A note on Sverdrup balance in the Southern Ocean. *J. Mar. Res.*, **40** (Suppl), 21–26..

Bryan, F., 1987: Parameter sensitivity of a primitive equation ocean general circulation model. *J. Phys. Oceanogr.*, **17,** 970–985.. Find this article online

Bryan, K., and L. J. Lewis, 1979: A water mass model of the world ocean. *J. Geophys. Res.*, **84,** 2503–2517..

Charney, J. G., and J. G. DeVore, 1979: Multiple flow equilibria in the atmosphere and blocking. *J. Atmos. Sci.*, **36,** 1205–1216.. Find this article online

Danabasoglu, G., and J. McWilliams, 1995: Sensitivity of the global ocean circulation to parameterizations of mesoscale tracer transports. *J. Climate*, **8,** 2967–2987.. Find this article online

Gent, P. R., W. G. Large, and F. O. Bryan, 2000: What sets the mean transport through Drake Passage? *J. Geophys. Res.*, in press..

Gill, A. E., and K. Bryan, 1971: Effects of geometry on the circulation of a three-dimensional Southern Hemisphere ocean model. *Deep-Sea Res.*, **18,** 685–721..

Gille, S. T., 1997: The Southern Ocean momentum balance: Evidence for topographic effects from numerical model output and altimeter data. *J. Phys. Oceanogr.*, **27,** 2219–2232.. Find this article online

— ,and K. A. Kelly, 1996: Scales of spatial and temporal variability in the Southern Ocean. *J. Geophys. Res.*, **101,** 8759–8773..

Gnanadesikan, A., 1999: A simple predictive model for the structure of the oceanic pycnocline. *Science*, **283,** 2077–2079..

Hallberg, R., 1995: Some aspects of the circulation in ocean basins with isopycnal intersecting the sloping boundaries. Ph.D. dissertation, University of Washington, 244 pp..

— ,1997: Localized coupling between surface and bottom-intensified flows over topography. *J. Phys. Oceanogr.*, **27,** 977–998.. Find this article online

Hellerman, S., and M. Rosenstein, 1983: Normal monthly wind stress over the world ocean with error estimates. *J. Phys. Oceanogr.*, **13,** 1093–1104.. Find this article online

Hughes, C. W., 1997: Comments on “On the obscurantist physics of form drag in theorizing about the Circumpolar Current.” *J. Phys. Oceanogr.*, **27,** 209–210.. Find this article online

Hughes, T. M. C., and A. J. Weaver, 1994: Multiple equilibria of an asymmetric two-basin model. *J. Phys. Oceanogr.*, **24,** 619–637.. Find this article online

Johnson, G. C., and H. Bryden 1989: On the strength of the Circumpolar Current. *Deep-Sea Res.*, **36,** 39–53..

Kalnay, E., and Coauthors, 1996: The NCEP/NCAR 40-Year Reanalysis Project. *Bull. Amer. Meteor. Soc.*, **77,** 437–471.. Find this article online

Kawase, M., 1987: Establishment of deep ocean circulation driven by deep-water production. *J. Phys. Oceanogr.*, **17,** 2294–2317.. Find this article online

Killworth, P. D., and M. M. Nanneh, 1994: Isopycnal momentum budget of the Antarctic Circumpolar Current in the Fine Resolution Antarctic Model. *J. Phys. Oceanogr.*, **24,** 1203–1224.. Find this article online

Krupitsky, A., and M. A. Cane, 1994: On topographic pressure drag in a zonal channel. *J. Mar. Res.*, **52,** 1–22..

— ,V. M. Kamenkovich, N. Naik, and M. A. Cane, 1996: A linear equivalent barotropic model of the Antarctic Circumpolar Current with realistic coastlines and bottom topography. *J. Phys. Oceanogr.*, **26,** 1803–1824.. Find this article online

Marshall, J., D. Olbers, H. Ross, and D. Wolf-Gladrow, 1993: Potential vorticity constraints on the dynamics and hydrography of the Southern Ocean. *J. Phys. Oceanogr.*, **23,** 465–487.. Find this article online

McDermott, D., 1996: The regulation of Northern Hemisphere overturning by Southern Hemisphere winds. *J. Phys. Oceanogr.*, **26,** 1234–1255.. Find this article online

Mestaz-Nunez, A. M., D. B. Chelton, and R. A. DeSzoeke, 1992: Evidence of time-dependent Sverdrup circulation in the South Pacific from the Seasat scatterometer and altimeter. *J. Phys. Oceanogr.*, **22,** 934–943.. Find this article online

Munk, W., and A. Palmen, 1951: Note on the dynamics of the Antarctic Circumpolar Current. *Tellus,* **3,** 53–55..

Olbers, D., 1998: Comments on "On the obscurantist physics of 'form drag' in theorizing about the Circumpolar Current." *J. Phys. Oceanogr.*, **28,** 1647–1654.. Find this article online

— ,and C. Völker, 1996: Steady states and variability in oceanic zonal flows. *Decadal Climate Variability*, D. L. T. Anderson and J. Willebrand, Eds., NATO ASI Ser. I, Vol. 44, Springer-Verlag, 407–433..

Orsi, A. H., T. Whitworth III, and W. D. Nowlin, 1995: On the meridional extent and fronts of the Antarctic Circumpolar Current. *Deep-Sea Res. I,* **42,** 641–673..

Pacanowski, R. C., 1996: MOM 2 documentation, user's guide and reference manual. GFDL Ocean Tech. Rep. 3.1, Geophysical Fluid Dynamics Laboratory, NOAA, 329 pp. [Available from GFDL, P.O. Box 308, Princeton, NJ 08542.].

Park, Y. G., and K. Bryan, 2000: Comparison of thermally driven circulations from a depth-coordinate model and an isopycnal layer model. Part I: A scaling-law sensitivity to vertical diffusivity. *J. Phys. Oceanogr.*, **30,** 590–605.. Find this article online

Saunders, P., and S. R. Thompson, 1993: Transport, heat and freshwater fluxes within a diagnostic numerical model (FRAM). *J. Phys. Oceanogr.*, **23,** 452–464.. Find this article online

Stevens, D. P., and V. O. Ivchenko, 1997: The zonal momentum balance in an eddy-resolving general circulation model of the Southern Ocean. *Quart. J. Roy. Meteor. Soc.*, **123,** 929–951..

Stommel, H., 1957: A survey of ocean current theory. *Deep-Sea Res.*, **4,** 149–184..

— ,1961: Thermohaline convection with two stable regimes of flow. *Tellus,* **13,** 224–230..

Straub, D., 1993: On the transport and angular momentum balance of channel models of the Antarctic Circumpolar Current. *J. Phys. Oceanogr.*, **23,** 776–782.. Find this article online

Sverdrup, H. U., M. W. Johnson, and R. H. Fleming, 1942: *The Oceans: Their Physics, Chemistry and Biology.* Prentice-Hall, 620 pp..

Thompson, S. R., 1993: Estimation of the transport of heat in the Southern Ocean using a fine-resolution numerical model. *J. Phys. Oceanogr.*, **23,** 2493–2497.. Find this article online

Toggweiler, J. R., and B. Samuels, 1993: New radiocarbon constraints on the upwelling of abyssal water to the ocean's surface. *The Global Carbon Cycle,* M. Heimann, Ed., Springer-Verlag, 333–365..

— ,and — ,1995: Effect of Drake Passage on the global thermohaline circulation. *Deep-Sea Res.*, **42,** 477–500..

— ,and — ,1998: On the ocean's large-scale circulation near the limit of no vertical mixing. *J Phys. Oceanogr.*, **28,** 1832–1852..

Völker, C., 1999: Momentum balance in zonal flows and resonance of baroclinic Rossby waves. *J. Phys. Oceanogr.*, **29,** 1666–1681.. Find this article online

Wang, L., 1994: A linear homogeneous channel model for topographic control of the Antarctic Circumpolar Current. *J. Mar. Res.*, **52,** 649–685..

— , and R. X. Huang, 1995: A linear homogeneous model of wind-driven circulation in a β-plane channel. *J. Phys. Oceanogr.*, **25,** 587–603.. Find this article online

Warren, B., 1990: Suppression of deep oxygen concentrations by Drake Passage. *Deep-Sea Res.*, **37,** 1899–1907..

— , J. LaCasce, and P. A. Robbins, 1996: On the obscurantist physics of "form drag" in theorizing about the Circumpolar Current. *J. Phys. Oceanogr.*, **26,** 2297–2301.. Find this article online

Wells, N. C, and B. A. DeCuevas, 1995: Depth-integrated vorticity budget of the Southern Ocean from a general circulation model. *J. Phys. Oceanogr.*, **25,** 2569–2582.. Find this article online

Whitworth, T., III, 1983: Monitoring the transport of the Antarctic Circumpolar Current at Drake Passage. *J. Phys. Oceanogr.*, **13,** 2045–2057.. Find this article online

— , W. D. Nowlin, and S. J. Worley, 1982: The net transport of the Antarctic Circumpolar Current through Drake Passage. *J. Phys. Oceanogr.*, **12,** 960–971.. Find this article online

Wright, D. G., T. F. Stocker, and D. Mercer, 1998: Closures used in zonally averaged ocean models. *J. Phys. Oceanogr.*, **28,** 791–804.. Find this article online

---

Tables

Table 1. Wind stresses and ACC transport for the simple models with damping. Columns show average wind stress, wind stress at the northern edge of the channel, wind stress at the southern edge of the channel, modeled ACC transport, transport due to lower layer pressure gradients, transport in the upper layer relative to the lower layer, and predicted transport in the upper layer relative to the lower layer from (9).

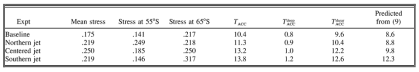

Expt	Mean stress	Stress at 55°S	Stress at 65°S	T_{ACC}	T^{low}_{ACC}	T^{new}_{ACC}	Predicted from (9)
Baseline	.175	.141	.217	10.4	0.8	9.6	8.6
Northern jet	.219	.249	.218	11.3	0.9	10.4	8.8
Centered jet	.250	.185	.250	13.2	1.0	12.2	9.8
Southern jet	.219	.146	.317	13.8	1.2	12.6	12.3

Click on thumbnail for full-sized image.

Table 2. Sensitivity of shear and deep transport to changes in model framework.

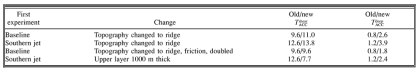

First experiment	Change	Old/new T^{low}_{ACC}	Old/new T^{low}_{DR}
Baseline	Topography changed to ridge	9.6/11.0	0.8/2.6
Southern jet	Topography changed to ridge	12.6/13.8	1.2/3.9
Baseline	Topography changed to ridge, friction, doubled	9.6/9.6	0.8/1.8
Southern jet	Upper layer 1000 m thick	12.6/7.7	1.2/2.4

Click on thumbnail for full-sized image.

Table 3. Summary of the different model wind fields and their effect on various quantities.

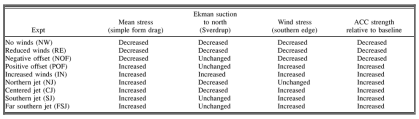

Expt	Mean stress (simple form drag)	Ekman suction to north (Sverdrup)	Wind stress (southern edge)	ACC strength relative to baseline
No winds (NW)	Decreased	Decreased	Decreased	Decreased
Reduced winds (RE)	Decreased	Decreased	Decreased	Decreased
Negative offset (NOF)	Decreased	Unchanged	Decreased	Decreased
Positive offset (POF)	Increased	Unchanged	Increased	Increased
Increased winds (IN)	Increased	Increased	Increased	Increased
Northern jet (NJ)	Increased	Decreased	Unchanged	Increased
Centered jet (CJ)	Increased	Decreased	Increased	Increased
Southern jet (SJ)	Increased	Unchanged	Increased	Increased
Far southern jet (FSJ)	Increased	Unchanged	Increased	Increased

Click on thumbnail for full-sized image.

Table 4. Dependence of ACC transport on mean wind stress, wind stress at northern edge of the channel, and wind stress at the southern edge of the channel for the global MOM runs.

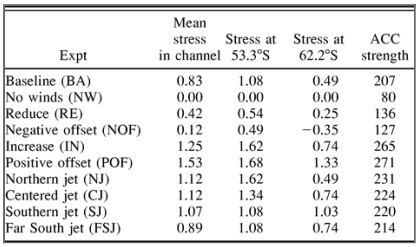

Expt	Mean stress in channel	Stress at 53.3°S	Stress at 62.2°S	ACC strength
Baseline (BA)	0.83	1.08	0.49	207
No winds (NW)	0.00	0.00	0.00	80
Reduce (RE)	0.42	0.54	0.25	136
Negative offset (NOF)	0.12	0.49	−0.35	127
Increase (IN)	1.25	1.62	0.74	265
Positive offset (POF)	1.53	1.68	1.33	271
Northern jet (NJ)	1.12	1.62	0.49	231
Centered jet (CJ)	1.12	1.34	0.74	224
Southern jet (SJ)	1.07	1.08	1.03	220
Far South jet (FSJ)	0.89	1.08	0.74	214

Click on thumbnail for full-sized image.

Table 5. Leading terms in the zonal momentum balance in the Drake Passage latitudes for three different models, for the uppermost 50 m, 50–2000 m, and 2000–5000 m. For each depth range, the horizontally and vertically integrated Coriolis acceleration (in $m^3\ s^{-2}$) is shown along with the dominant term balancing it. Note that the balance in the top 50 m is largely between Coriolis force and vertical diffusion (so that Ekman layer dynamics dominate). In the interior above the sill depth meridional diffusion of momentum is the dominant term balancing cross-channel flow, but the total is relatively small. At depth,

the dominant balance is between cross-ridge pressure gradients (form drag) and Coriolis forces.

	Case name		
	BA	RE	NOF
ACC transport (Sv)	207	136	127
X-momentum balance (0–50 m)			
Eastward Coriolis acceleration	−1427	−714	−467
Vertical diffusion	1432	716	470
X-momentum balance (50–2000 m)			
Eastward Coriolis acceleration	189	86	92
Meridional diffusion	−184	−85	−88
X-momentum balance (2000–5000 m)			
Coriolis acceleration	1238	627	375
Pressure gradient	−1132	−556	−275
Depth-averaged balance			
Pressure gradient/wind stress	0.79	0.78	0.59
Meridional diffusion/wind stress	0.18	0.18	0.33

Click on thumbnail for full-sized image.

Figures

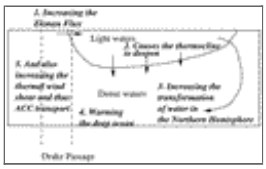

Click on thumbnail for full-sized image.

Fig. 1. A conceptual picture of how Southern Hemisphere winds change the depth of the pycnocline, the Northern Hemisphere overturning, and the ACC transport.

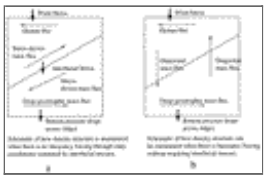

Click on thumbnail for full-sized image.

Fig. 2. Illustration of two extreme cases illustrating the relationship between the zonal momentum balance and buoyancy forcing. Light arrows represent mass fluxes. Heavy arrows represent momentum fluxes. (a) A case where there is no diapycnal mass flux between the light and dense layers. In order to establish a steady state, momentum must be fluxed from the upper layer to the lower layer and the mass fluxes generated by the stress between layers must balance the surface Ekman flux and the deep geostrophic mass flux below the ridges. (b) A case where buoyancy forcing allows for diapycnal mass fluxes between the upper and lower layers. This case does not require interfacial stresses to close the momentum balance. Note that in both cases, averaging vertically will yield a balance between wind stress and “form drag.”

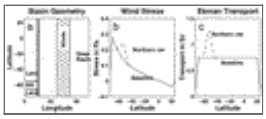

Click on thumbnail for full-sized image.

Fig. 3. Schematic of the simple model runs. (a) Model geometry. The basin is reentrant over the sill between 55° and 65°S. The sill depth is 2000 m and the deep basin is 4000 m deep. Winds are applied within the deep basin only over the hatched portion. (b) Wind stress within the forcing region for two cases, the baseline case with constant Ekman transport everywhere except near the boundaries, and the northern jet case, with a jet of winds centered at 55°S. (c) Ekman transport (in Sv) for the two cases in (c).

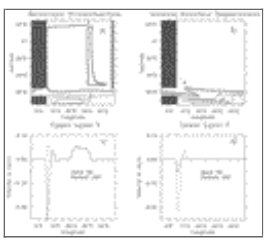

Click on thumbnail for full-sized image.

Fig. 4. Solution for the baseline case with interfacial damping. (a) Barotropic streamfunction (in Sv). (b) Interface height displacement (in m). (c) Upper layer meridional velocity at 5°N and 35°S. (d) Lower layer meridional velocity at 5°N and 35°S.

Click on thumbnail for full-sized image.

Fig. 5. Internal interface height displacement averaged across the center of the basin for the runs with interfacial restoring. Dashed lines are predicted height displacements from (7) and (8). Chain-dotted lines mark the latitudes of the channel edges.

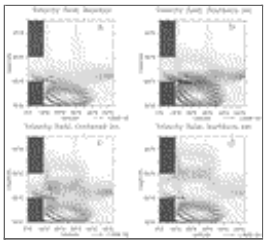

Click on thumbnail for full-sized image.

Fig. 6. Velocity fields for the four runs with interfacial damping. Standard vector is 0.015 m s^{-1}. (a) Baseline case, (b) southern jet, (c) centered jet, and (d) northern jet.

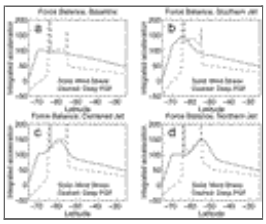

Click on thumbnail for full-sized image.

Fig. 7. Balance between the wind stress (solid lines) and the pressure gradient below 2000 m depth (dashed lines) for the four runs with interfacial damping, demonstrating that within the latitudes of the passage (65° to 55°S) these two terms are largely in balance. Strong frictional ageostrophic effects are seen at the edges of the passage. (a) Baseline case, (b) southern jet case, (c) centered jet case, and (d) northern jet case.

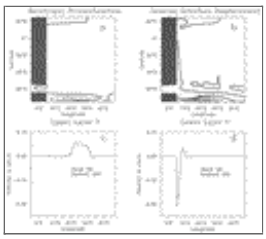

Click on thumbnail for full-sized image.

Fig. 8. Same as Fig. 4 but with fixed sources and sinks instead of interfacial damping.

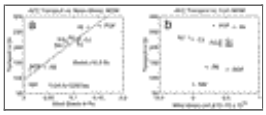

Click on thumbnail for full-sized image.

Fig. 9. Regression of the ACC and deep transport in the global runs vs wind stresses. (a) ACC transport vs mean wind stress in channel. (b) ACC transport vs wind stress curl at 51.1°S.

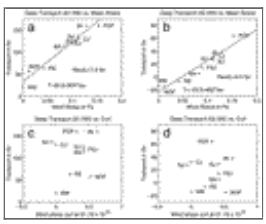

Click on thumbnail for full-sized image.

Fig. 10. Regression of the deep transport at two locations vs wind stress and wind stress curl. (a) Deep transport at 67.5°W (in Drake Passage) vs mean wind stress in channel latitudes. (b) Deep transport at 52.5°W vs mean wind stress. (c) Deep transport at 67.5°W transport vs wind stress curl at 51.1°S. (d) Deep transport at 52.5°W vs wind stress curl at 51.1°S.

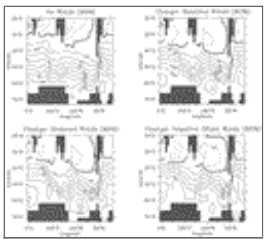

Click on thumbnail for full-sized image.

Fig. 11. Barotropic streamfunction (in Sv) from four runs of the modular ocean model. (a) No wind stress (buoyancy forcing only case NW). (b) Change from no winds with winds given by Hellerman and Rosenstein (1983) (baseline winds case, BA). (c) Change from no winds, winds south of 30°S reduced by 50% (reduced winds case, RE). (d) Change from no winds, baseline winds plus a negative offset (negative offset case, NOF).

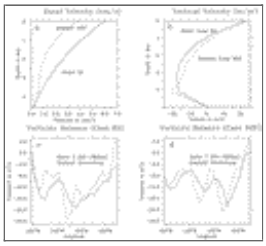

Click on thumbnail for full-sized image.

Fig. 12. Velocity changes between the baseline (BA) and negative offset cases (NOF). (a) Averaged zonal velocity at 57.8°S, 160°–90°W (SE Pacific). (b) Averaged vertical velocity from 60° to 55°S. Note that the changes are zero at the upper boundary (where Ekman pumping is important) and relatively small elsewhere in the water column. (c) Geostrophic vorticity balance along 57.8°S for baseline case. Solid line is integrated southward transport from 55 to 1895 m. Dashed line is $f/\beta(w|_{55\mathrm{m}} - w|_{1895\mathrm{m}})$, the transport associated with vortex stretching. (d) Geostrophic vorticity balance for case NOF. Note that there are differences, due to changes in the deep overturning, but that the overall level of transport is similar.

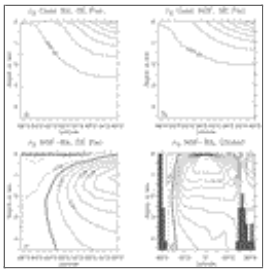

Click on thumbnail for full-sized image.

Fig. 13. Illustration of how the density structure changes between the baseline and negative offset case:(a) σ_0 for the baseline case in the southeast Pacific, (b) σ_0 for the negative offset case, (c) difference in σ_0 for the southeast Pacific (negative offset − baseline), and (d) globally averaged difference in σ_0, (negative offset − baseline).

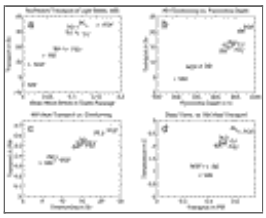

Click on thumbnail for full-sized image.

Fig. 14. How Southern Ocean winds produce changes in the ACC: (a) Northward transport of light ($\sigma_0 < 27.2$) water vs average wind stress in Drake Passage. Note that there is a general trend that as the wind stress increases, the northward transport of light water increases. (b) NH overturning vs pycnocline depth. Note that as the northward transport of light water increases, so does (in general) the overturning. (c) Northward heat transport vs overturning. As the overturning increases, it transports more and more heat northward, so that more water is being transformed. The range of the temperature transformation in the model is about 7.5°C. (d) Increase in deep temperatures just to the north of the ACC correlated with Northern Hemisphere heat transport. The temperatures to the south change little.

Corresponding author address: Dr. Anand Gnanadesikan, NOAA/GFDL and AOS Program, Princeton University, 302 Sayre Hall, Post Office Box CN710, Princeton, NJ 08544-0710.

E-mail: gnana@princeton.edu

top